Original Research Article

Transfer Matrix Modeling Optical Properties of Short-Period Aluminum Oxide-Copper Multi-Layered Nanocomposites

Abstract:

This research delves into applying Sputtering Atomic Layer Augmented Deposition (SALAD) to create thin aluminum oxide and copper films. SALAD combines atomic layer deposition (ALD) techniques, providing precise film thickness control. The study utilizes the transfer matrix method to analyze the reflectance, aiming to gain insights into the interactions between the constituent materials. The researchers generated samples consisting of 300 layers of AlO_x and Cu, which were then analyzed using spectroscopic ellipsometry. Distinct functions were developed to represent the equations for transmission matrices and propagation matrices. To evaluate our approach, four pairs of HfO_2 and SiO_2 thin film layers were simulated, with their refractive indices derived from Sellmeier's equations, which was found to be very successful. Although the simulation successfully predicted reflectance for systems, there were variations compared to the laboratory results obtained for the more complex AlO_x-Cu samples. Polynomial functions were used to model these differences, suggesting that factors like unaccounted plasmonics and layer imperfections may be at play. This study lays a foundation for research to refine models and explore quantum effects that influence these advanced materials.

Keywords : Mathematics, Transfer Matrix Method, Optics, Physics, Computer Simulation

Introduction:

Research involving the intersection of diverse disciplines has often uncovered unique phenomena tied to the quantum characteristics of materials. Giraldo et al. stated that the refinement of synthesis techniques is undervalued, yet, engineering methods can produce materials with unprecedented structural intricacies[1]. Thus, Giraldo et al. used a hybrid thin-film deposition system, termed sputtering atomic layer augmented deposition (SALAD), which is based on both sputtering, physical vapour deposition, (SPU) and atomic layer deposition, chemical vapour deposition, (ALD) techniques[1]. They used this technique as in traditional systems, SPU and ALD operate separately or in cluster tools specifically designed for either SPU or ALD[1]. However, a new approach allows SPU and ALD to function in the same environment, processes that nearly follow one after the other from the two deposition methods. This enables near-simultaneous or consecutive processes, even though these two deposition methods are typically seen as incompatible[1]. Although two methods seemed incompatible, this approach shows a novel application that could not be produced before. A case showcasing the special capabilities of SALAD features a thin-film configuration, which is made up of aluminum oxide (AlO_x) and copper (Cu), used; in order to emphasize the unique capabilities of SALAD in combining thin-film materials that are typically challenging to prepare using a singular deposition method like SPU or ALD, AlO_x, and Cu were specifically selected, as Cu is widely used in ALD[1,2,3,4]. In the SALAD system, using SPU puts down material quickly, and thus, it can be hard to control the exact thickness, which also varies with applied voltage[1]. ALD, on the other hand, always puts down one atom layer every cycle. Hence, the total thickness is very easy to control[1].

In this study, we attempted to model the samples' spectral reflectance using the transfer-matrix method, simplifying calculating total reflectance. This study aims to gain a deeper understanding of samples with spectral reflectance that does not appear to represent the constituent materials. We attempted to make the model work; then, we could have predicted material properties without making and testing samples.

Experiment

Using SALAD, samples were made with 300 layers, as seen in Figure 1. Each pair had an ALD-deposited AlO_x layer of about 39 nm and a sputtered Cu layer of 15 to 84 nm thick[1,5]. After being examined with spectroscopic ellipsometry, the samples showed reflectance patterns that weren't just a straightforward mix of their base materials[5].

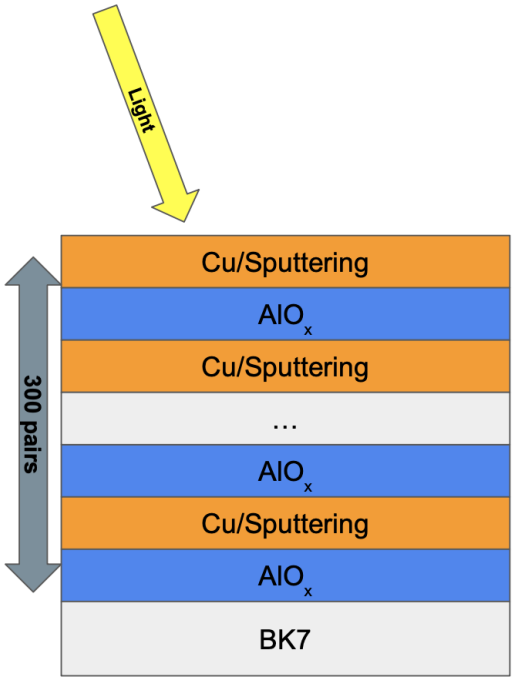

Figure 1: Thin films 300 layers

The transfer matrix method was used to model the sample of the short-period AlOx-Cu multi-layered nanocomposite. The magnitude of the electric field of incident light is noted as "Light" in the figure.

AlO_x was selected since it is mature as a dielectric material, which is deposited by ALD (ALD-AlO_x). Cu, often deposited by SPU (SPU-Cu), was the preferred metallic material. The potential oxides formed from Cu, such as cuprous and cupric oxides, can be clearly differentiated from AlO_x, simplifying theoretical analysis. The ALD-AlOx had a self-limiting deposition rate of 0.13nm/cycle[1,5]. In contrast, the rate for SPU-Cu was adjusted to 0.04 nm/s with the specific Cu sub-layer content being controlled by setting a distinct time, t_{SPU} for SPU-Cu. In one SALAD cycle, there is an $Al(CH_3)_3$ pulse, followed by its purge, then an H_2O pulse, and its subsequent purge, ending with Cu sputtering for a specific t_{SPU} duration[1,5]. By repeating the SALAD cycle 300 times for specific t_{SPU}multiple samples, each with varying Cu content, were created. All the depositions took place at 150°C with pressures ranging from 18.66-32.00 Pa, much lower than the pressure that people experience at sea level[1,5]. The samples underwent spectroscopic reflectometry using the FilmTek 4000 spectroscopic reflectometer, measuring the change in s-polarized light to determine reflectance with a 70° incident angle.

Results and Discussion

Matlab was used to simulate the experiment. To test the methodology, we modeled 4 pairs of HfO_2 and SiO_2 thin film layers with refractive indexes generated from Sellmeier's equations, which gives the reflectance as a function of wavelength as shown in Equation 1. The incident angle was set at 0 degrees, with the HfO_2 layers at 59 nm wide and Al_2O_3 layers at 71 nm wide. The results are shown in Figure 2 where it is compared to known results.

$$n^2(\lambda) = 1 + \frac{a_1\lambda^2}{\lambda^2 - b_1} + \frac{a_2\lambda^2}{\lambda^2 - b_2} + \frac{a_3\lambda^2}{\lambda^2 - b_3} \qquad \text{Equation 1}$$

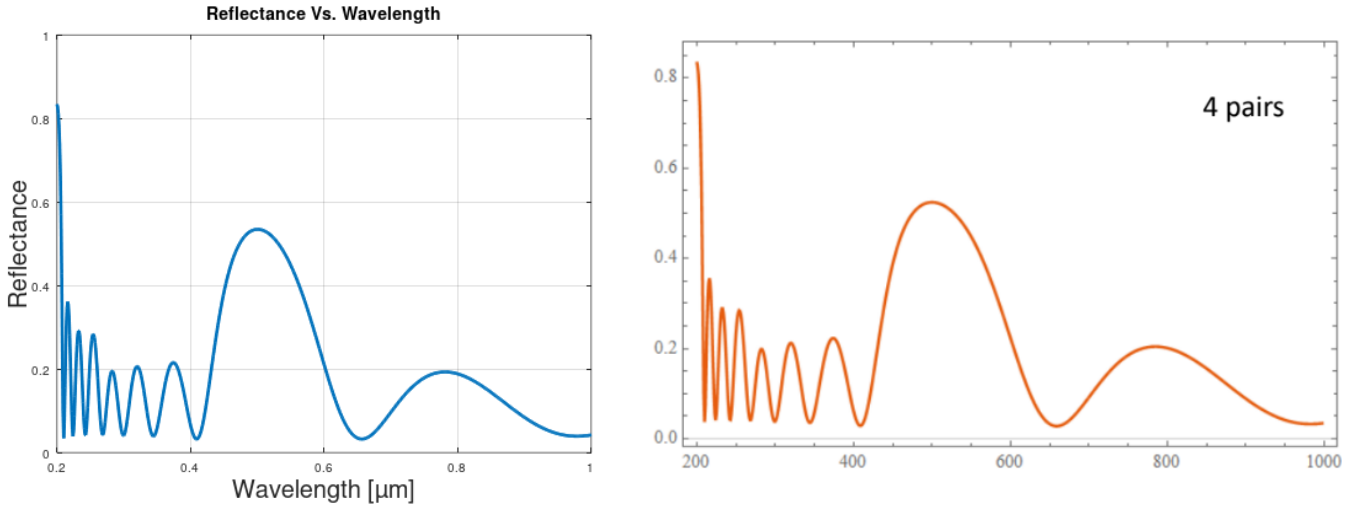

A) Modeled that was simulated using Transfer Matrix Method with MatLab,

B) Known reflectance

Figure 2: 4 pair HfO_2 and Al_2O_3 simulation results

Looking at graph A from Figure 2, our modeled reflectances of 4 pairs of HfO_2 and Al_2O_3 matches graph B, which were known results. Not only did the general shape match, but the exact values match as well which is significant because in failed simulations with faulty code, the general curve and shape of the graph would match up, however the graph would be too low or too high. Since this example clearly worked, we began to work on the full 300 layers of Cu and AlO_x, however the Sellmeier's equation cannot be used in the actual sample because it only holds true for bulk films, and does not work for the thin films the samples are. In the experiment, previously observed data for the thin films of Cu and AlO_x was used[6]. For the experiment, the incident angle was 70° with the distance of AlO_x at 39 nm, and Cu layers tested at 15 nm, 24 nm, 36 nm, 48 nm, 60 nm, 72 nm and 84 nm, as per the SALAD samples. In the experiment, the variable *m* represents the percent of the sample comprised of copper.

After attaining all variables used in the transmission and propagation matrices, they were multiplied together to form matrix M (Equation 18).

Where 0 represents air, 1 represents Cu thin film, 2 represents AlO_x thin film, and 3 represents BK7. After this, the code calculates the reflectance by dividing $M_{(2,1)}$ by $M_{(1,1)}$. The code was run over the range of wavelengths 200 nm to 1500 nm for all the samples, yielding Figure 3A.

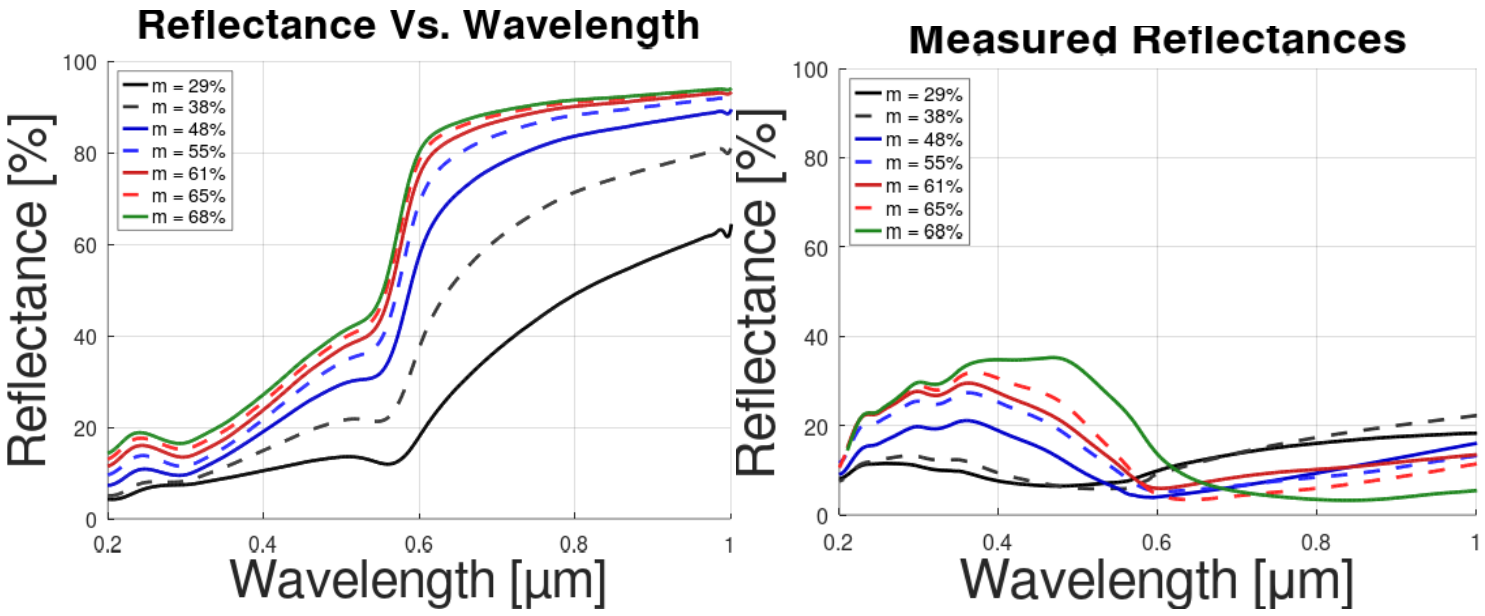

A: Results of 300 layer simulation **B:** Observed results from lab

Figure 3: Simulation results compared with lab results of reflectances from 300 Cu AlO_x pairs where *m* represents the percent of sample made up of copper.

In Figure 3A, there is a slight bump at around 0.2-0.3 μm, followed by a steady increase. From about 0.5 μm to 0.7 μm, there appears to be a sudden increase in reflectance calculated. As for Figure 3B, all the samples consistently show a wide peak. The samples typically exhibit a rise in reflectance below 0.4 μm, marked by a dip in reflectance near 0.5-0.6 μm. Interestingly, this characteristic doesn't seem inherent to either Cu or AlO_x-Cu[6]. The distinctive combination of AlOx and Cu, a method facilitated by SALAD, is observed in Figure 3B, which is an unusual feature[6]. However, if analyzed individually, both AlO_x and Cu would likely present expected and predictable reflectance spectra[6]. If Cu predominantly influenced the construction of the spectra, absorption linked to its bulk plasmon polariton would emerge[6]. Yet, all the spectra consistently present a pronounced dome-like curvature accompanied by a steep rise but with a lower range. The significant rise previously mentioned causes a clear decrease in reflectance within that energy range, which is lower than what would be expected for AlO_x. Beyond the influence of plasmon polaritons, particles that consist of a photon in strong coupling with an electric dipole form a hybrid structure, there seems to be a shifting dominance between AlO_x and Cu across the energy spectrum; specifically, SPU-Cu takes a more dominant role in the higher energy range.

Looking at Figure 3A compared with Figure 3B, it is clear that the simulation results do not match the observed results, suggesting that there are factors unaccounted for within the simulation. Temperature, pressure, or other environmental conditions could affect the material properties and thus the results. We decided to model the relationship between our simulated results and the observed results to possibly narrow down why our model is mathematically failing. To do this, we generated 11th degree polynomial functions to model both of the graphs, then used basic division to figure out the relationship. Figure 4 displays the ratios for each of the samples.

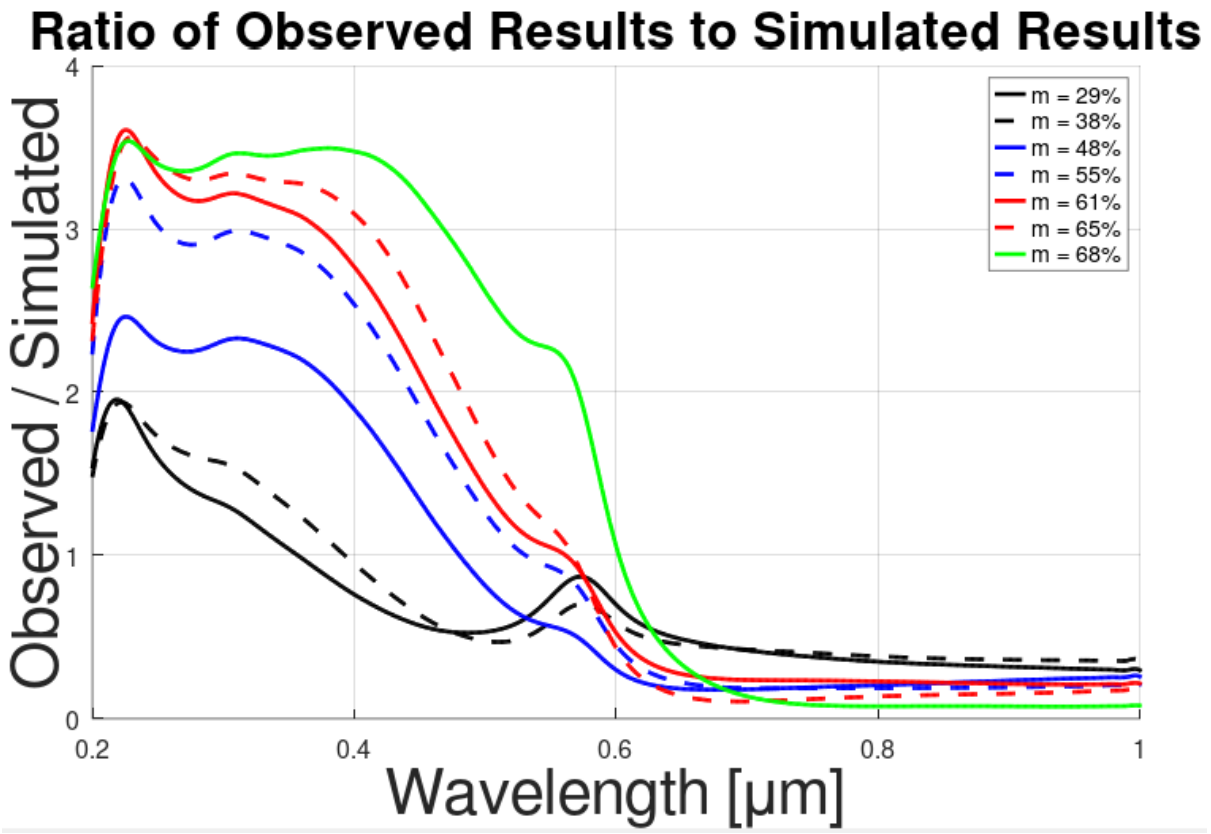

Figure 4: Observed results divided by simulated results at varying wavelengths of light from 200 nm to 1000nm.

Figure 4 demonstrates that from the ranges 200 nm to around 500 nm of light, the simulation is lower than the observed results while in the wavelengths longer than that it appears the simulation is larger than the observed results. However, there does seem to be a consistent pattern across the different samples, which we can try to model by generating a mathematical expression that evaluates to the coefficient as a function of wavelength and thickness. From this, we may be able to determine which phenomena match the described effect.

$p_1(m) = -2.5482e\text{-}34m^5 + 6.1582e\text{-}32m^4 - 5.1994e\text{-}30m^3 + 1.8123e\text{-}28m^2 - 2.2293e\text{-}27m + 1.3438e\text{-}27$

$p_2(m) = 2.2225e\text{-}30m^5 - 5.3777e\text{-}28m^4 + 4.5499e\text{-}26m^3 - 1.5907e\text{-}24m^2 + 1.9633e\text{-}23m - 1.1759e\text{-}23$

$p_3(m) = -8.4678e\text{-}27m^5 + 2.0517e\text{-}24m^4 - 1.74e\text{-}22m^3 + 6.1037e\text{-}21m^2 - 7.5632e\text{-}20m + 4.5154e\text{-}20$

$p_4(m) = 1.8503e\text{-}23m^5 - 4.4899e\text{-}21m^4 + 3.8178e\text{-}19m^3 - 1.3444e\text{-}17m^2 + 1.6735e\text{-}16m - 1.0007e\text{-}16$

$p_5(m) = -2.5594e\text{-}20m^5 + 6.221e\text{-}18m^4 - 5.3052e\text{-}16m^3 + 1.8762e\text{-}14\ m^2 - 2.3478e\text{-}13m + 1.4154e\text{-}13$

$p_6(m) = 2.3336e\text{-}17m^5 - 5.6824e\text{-}15m^4 + 4.8612e\text{-}13m^3 - 1.7273e\text{-}11m^2 + 2.1747e\text{-}10m - 1.3332e\text{-}10$

$p_7(m) = -1.4154e\text{-}14m^5 + 3.453e\text{-}12m^4 - 2.9638e\text{-}10\,m^3 + 1.0585e\text{-}08m^2 - 1.3418e\text{-}07m + 8.4507e\text{-}08$

$p_8(m) = 5.6215e\text{-}12m^5 - 1.3739e\text{-}09m^4 - 1.1831e\text{-}07m^3 - 4.2473e\text{-}06m^2 + 5.4242e\text{-}05m - 3.5476e\text{-}05$

$p_{9,}(m) = -1.3957e\text{-}09m^5 + 3.4161e\text{-}07m^4 - 2.95e\text{-}05m^3 - 0.0010642m^2 - 0.013696m + 0.0093889$

$p_{10}(m) = 1.9503e\text{-}07m^5 - 4.7786e\text{-}05m^4 + 0.0041351m^3 - 0.14978m^2 + 1.9415m - 1.4065$

$p_{11}(m) = -1.1513e\text{-}05m^5 + 0.0028237m^4 - 0.24479m^3 + 8.8994m^2 - 116.18m + 91.536$

$c(m, \lambda) = p_1(m)\lambda^{10} + p_2(m)\lambda^9 + p_3(m)\lambda^8 + p_4(m)\lambda^7 + p_5(m)\lambda^6 + p_6(m)\lambda^5 + p_7(m)\lambda^4 + p_8(m)\lambda^3 + p_9(m)\lambda^2 + p_{10}(m)\lambda + p_{11}(m)$

Taking the different observed data points with different percentages of copper, polynomial equations were generated to model how the graph of coefficients behave at different wavelengths. The equation c takes variables m, the percentage of the sample composed of copper and λ, the wavelength being examined. The coefficients of the polynomials are individual polynomial functions as a function of m, and are only to the 5th power because we only had 7 data points to work with.

With this equation, we may be able to narrow down what factors are causing the discrepancies. Many quantum effects could impact our results, for example plasmonics. Some plasmonics are taken into consideration with the transfer matrix method, but the unaccounted for plasmonics, which include acoustic plasmonics among many others, could factor into the observed differences. Furthermore, the transfer matrix method assumes that each layer is perfectly flat, however in reality the layers are imperfect and rough, promoting further plasmonics effects. Another effect that could be responsible for the differences are interferences due to coupling between the copper layers relative to the distances between those layers, which in this case would be the thickness of AlO_x. The samples were designed to minimize interference, however some effects may still be present.

Methods

Plane Waves in Multilayer Films

In this section, the principles of reflectivity and transmissivity will be extended to films made up of m parallel layers of linear, isotropic media[7]. At each interface, the refraction index shifts suddenly in a step-wise manner, and the m-th layer possesses a consistent refraction index of n_m and a thickness of d_m. We will consider the refractive indices of the film layers and transmission medium as complex numbers, $n + ik$; this approach takes into consideration both the material's transmissivity and the absorption[7]. At every interface, the tangential component of the electric field must remain continuous per Maxwell's equations[8]. Just as in a single interface scenario, these boundary conditions necessitate the presence of both a "forward" and "back" propagating plane wave in each layer.

The equation below shows the Snell's law in a continuous layer:

$$n_0 sin(\theta_0) = n_1 sin(\theta_1) = n_2 sin(\theta_2) = \ldots = n_m sin(\theta_m) = n_{m+1} sin(\theta_{m+1}) \qquad \text{Equation 2}$$

The complex wave vectors are defined by the complex θ_m and the complex refractive indices[7]. If the incoming wave is s-polarized, then all the forward and reverse propagating fields in the film layers will also be s-polarized, and this can be derived from the breakdown of the complex angles.

The s-polarization reflectivity of the film is:

$$r_s \equiv \frac{E_s^{(r)}}{E_s^{(i)}} \quad \text{Equation 3}$$

Also, the s-polarization transmittivity will be:

$$t_s \equiv \frac{E_s^{(t)}}{E_s^{(i)}} \quad \text{Equation 4}$$

Where, $E_s^{(i)}$ and $E_s^{(r)}$ are the electric field phasors of the s-polarized incident and reflected plane waves.

Single Layer Films

Optics textbooks derive single layer films through the summation of partial waves, where each incident plane wave at an interface leads to reflected and transmitted partial waves, a process that continues indefinitely at subsequent interfaces[7,8,9,10,11,12]. The Fresnel equations are used to calculate the reflectivities and transmissivities for a wave incident from medium to a homogeneous $m + 1$th sub-layer in relation to those of a mth sub-layer.

$$r_s^{(m,\,m+1)} = \frac{n_m cos(\theta_m) - n_{m+1} cos(\theta_{m+1})}{n_m cos(\theta_m) + n_{m+1} cos(\theta_{m+1})} \quad \text{Equation 5}$$

$$t_s^{(m,\,m+1)} = \frac{2n_m cos(\theta_m)}{n_m cos(\theta_m) + n_{m+1} cos(\theta_{m+!})} \quad \text{Equation 6}$$

We assume that incident light was s-polarized and $r_s^{(m,\,m+1)}$ is the reflection coefficient and $t_s^{(m,\,m+1)}$ is the transmission coefficient. Additionally, the Stokes relations link the $m + 1$ to m and m to $m + 1$ reflectivities and transmissivities:

$$r_{s|p}^{(m,\,m+1)} = - r_{s|p}^{(m+1,\,m)} \quad \text{Equation 7}$$

and

$$(r_{s|p}^{m,\,m+1})^2 + (t_{s|p}^{m,\,m+1})(t_{s|p}^{m+1,\,m}) \quad \text{Equation 8}$$

In these equations, $s|p$ shows the equation is either s or p polarized light. Besides the interface effects, as waves move through each layer, their amplitudes and phases undergo changes. Using figure 1 and previous interface reflectivity equations, we derived:

$$E_{s|p}^{(r)} = [r_{s|p}^{(01)} + (t_{s|p}^{(01)})(t_{s|p}^{(10)})(r_{s|p}^{(12)} exp(i2y) \sum_{a=0}^{\infty} [r_{s|p}^{(10)}\ r_{s|p}^{(12)} exp(i2y)]^a] E_{s|p}^{(i)} \quad \text{Equation 9}$$

Using the Stokes relations to simplify, we carry out the summation using the equations above.

$$r_{s|p} = \frac{r_{s|p}^{(01)} + r_{s|p}^{(12)} exp(iy)}{1 + r_{s|p}^{(01)} + r_{s|p}^{(12)} exp(i2y)} \qquad \text{Equation 10}$$

Summing the partial transmitted fields gives (7):

$$E_{s|p}^{(t)} = [t_{s|p}^{(01)} t_{s|p}^{(12)} exp(iy) \sum_{a=0}^{\infty} [r_{s|p}^{(10)} \; r_{s|p}^{(12)} exp(i2y)]^{a}] E_{s|p}^{(i)} \qquad \text{Equation 11}$$

Which simplies to:

$$t_{s|p} = \frac{t_{s|p}^{(01)} + t_{s|p}^{(12)} exp(iy)}{1 + t_{s|p}^{(01)} + t_{s|p}^{(12)} exp(i2y)} \qquad \text{Equation 12}$$

When we take the limit of the equation:

$$t_{s|p}^{(02)} = \frac{t_{s|p}^{(01)} + t_{s|p}^{(12)}}{1 + r_{s|p}^{(01)} + r_{s|p}^{(12)}} \qquad \text{Equation 13}$$

And

$$r_{s|p}^{(02)} = \frac{r_{s|p}^{(01)} + r_{s|p}^{(12)}}{1 + r_{s|p}^{(01)} + r_{s|p}^{(12)}} \qquad \text{Equation 14}$$

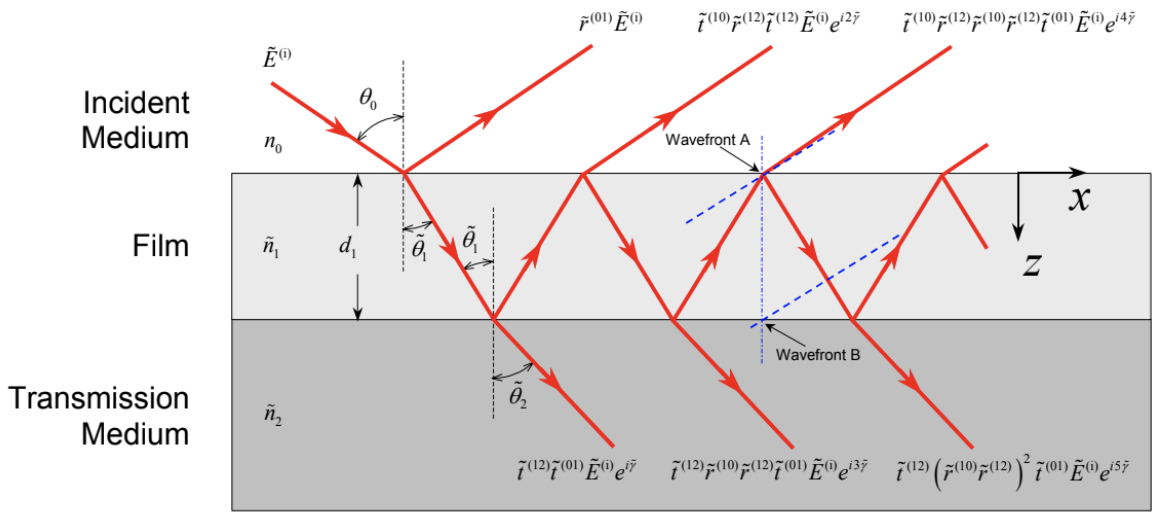

Figure 5: The reflectivity and transmissivity of a single-layer film through the use of Partial Waves[7].

Transfer Matrix Method

For a single layer, the approach of summing partial waves is accurate ((J. P. Landry. Optical oblique-incidence reflectivity difference microscopy: Application to label-free detection of reactions in biomolecular microarrays. Department of Physics, University of California, Davis (2008).)). However, its application becomes increasingly intricate with added layers. Given the linear nature of the Maxwell equations (pertaining to linear media) and the associated boundary stipulations, numerous transfer matrix methodologies have been established to compute the electromagnetic fields at distinct levels within layered media. The solution to the challenges presented by multi-layered systems is the usage of the dispersion matrix[8]:

$$D_{p|s}^{(m,m+1)} = \frac{1}{t_{p|s}^{(m,m+1)}} \begin{bmatrix} 1 & r_{p|s}^{(m,m+1)} \\ r_{p|s}^{(m,m+1)} & 1 \end{bmatrix} \quad \text{Equation 15}$$

$D_{p|s}^{(m,\,m+1)}$ is the dispersion matrix. For each layer, a $D_{p|s}^{(m,\,m+1)}$ matrix is produced. In our context, this means creating 300 such matrices. By multiplying these matrices, we can effectively gauge the cumulative light that passes through all 300 layers in the samples, as well as the total light reflected at the interface and any light linked to reflections at all other interfaces. However, this would lead to a model predicting infinite reflections due to lossless light. As such, another element to consider is the attenuation of light within a material, where its intensity diminishes in relation to the distance, d_m, that the light traverses[8]. The incoming light experiences attenuation proportional to $e^{i\gamma m}$, where γ_m denotes the propagation of the plane-wave along the z-direction. Modifying to express the attenuation in relation to all of the light (i.e., all of the transmission into and back-scattering at interfaces) traversing across the material results in[8]:

$$P_{p|s}^{(m)} = \begin{bmatrix} e^{-i\gamma m} & 0 \\ 0 & e^{i\gamma m} \end{bmatrix} \quad \text{Equation 16}$$

$$\gamma_m = 2\pi n_m \cos(\theta_m) \frac{d_m}{\lambda_0} \quad \text{Equation 17}$$

The variable θ_K represents the angle of incidence of the light at a given interface between sub-layers, measured in radians. The transfer matrix, M, is derived from the product of the transmission matrices and the propagation matrices, arranged in the sequence of the sub-layers[8].

$$M = D_{p|s}^{(0,\,1)} P_{p|s}^{(1)} D_{p|s}^{(1,\,2)} P_{p|s}^{(2)} (D_{p|s}^{(2,\,1)} P_{p|s}^{(1)} D_{p|s}^{(1,\,2)} P_{p|s}^{(2)})^{299} D_{p|s}^{(2,\,3)} \quad \text{Equation 18}$$

Where, 0 denotes air, 1 denotes Cu, 2 represents AlO_x, 3 denotes, optical quality glass sub-layers. The transfer matrix, when correlated with input light (E_{in}), reflected light (E_r), and transmitted light (E_T), yields the following relationship[8]:

$$\begin{bmatrix} E_{in} \\ E_r \end{bmatrix} = M \begin{bmatrix} E_t \\ 0 \end{bmatrix} \quad \text{Equation 19}$$

This can be rewritten as:

$$E_{in} = M_{11} E_t \quad \text{Equation 20}$$

$$E_r = M_{21} E_t \quad \text{Equation 21}$$

$$\frac{E_r}{E_{in}} = r = \frac{M_{21}}{M_{11}} \quad \text{Equation 22}$$

This suggests that the reflection coefficient, r, can be expressed as the ratio of the M_{21} element to the M_{11} element of the transfer matrix for a specified wavelength λ_0[8]. The nature of the incoming light and the reflected light is inconsequential. Their characteristics are not of primary concern, as the reflectivity is inherently a property of the material itself.

Conclusion

Nanocomposite samples of 300 AlO_x and Cu layers were made up using SALAD, which combines sputtering and ALD benefits in one vacuum chamber. We used the transfer matrix method to simulate the reflectance of these samples. The experiment was simulated using, employing custom functions for transmission and propagation matrices. The study successfully estimated spectral reflectance using the transfer-matrix method, and validated the approach with HFO_2 and SiO_2 thin film simulations based on Sellmeier's equations. The results differed from lab observations, prompting further analysis. We then simulated 300 layers of Cu and AlO_x, using variable incident angles and layer distances. The simulation and observed results were compared using polynomial functions to identify discrepancies. Factors like unaccounted plasmonics, layer imperfections, and inter-layer coupling could contribute to the observed differences. Future research aims to refine the mathematical model to account for these variables. The polynomial equations we developed to model the differences between simulated results offer a mathematical framework that could greatly contribute to future research. By understanding how the percentage of copper in a sample wavelength and observed discrepancies are related researchers might be able to identify phenomena or factors that are responsible for these patterns.

Reference

1. B. Giraldo, D. M. Fryauf, B. Cheney, J. H. Sands, N. P. Kobayashi. Demonstration of sputtering atomic layer augmented deposition: Aluminum oxide-copper dielectric-metal nanocomposite thin films. *ACS Applied Materials & Interfaces.* **12**, 14280–14288 (2020). https://doi.org/10.1021/acsami.9b18628

2. Z. Li, A. Rahtu, R. G. Gordon. Atomic layer deposition of ultrathin copper metal films from a liquid copper(I) amidinate precursor. *Journal of the Electrochemical Society*. **153**, C787 (2006). https://doi.org/10.1149/1.2338632

3. L. C. Kalutarage, S. B. Clendenning, C. H. Winter. Low-temperature atomic layer deposition of copper films using borane dimethylamine as the reducing co-reagent. *Chemistry of Materials: A Publication of the American Chemical Society*. **26**, 3731–3738 (2014). https://doi.org/10.1021/cm501109r

4. Z. Guo, H. Li, Q. Chen, L. Sang, L. Yang, Z. Liu, X. Wang. Low-temperature atomic layer deposition of high purity, smooth, low resistivity copper films by using amidinate precursor and hydrogen plasma. *Chemistry of Materials: A Publication of the American Chemical Society*. **27**, 5988–5996 (2015). https://doi.org/10.1021/acs.chemmater.5b02137

5. S. A. Tornøe, J. H. Sands, N. P. Kobayashi. Semiconductor-like optical properties unveiled by modeling of short-period aluminum oxide-copper multi-layered nanocomposites deposited by sputtering atomic layer augmented deposition (SALAD). *Arxiv.org*. Retrieved August 17, 2023, from http://arxiv.org/abs/2206.14013

6. M. R. Querry. Optical constants. Retrieved from https://apps.dtic.mil/sti/citations/ADA158623 (1985).

7. J. P. Landry. Optical oblique-incidence reflectivity difference microscopy: Application to label-free detection of reactions in biomolecular microarrays. Department of Physics, University of California, Davis (2008).

8. L. Z. Dissertation. Transparent boundary conditions for Maxwell's equations: Numerical concepts beyond the PML method. D-Nb.Info. Retrieved August 17, 2023, from https://d-nb.info/1023784203/34

9. E. Hecht. Optics. 3rd Edition, *Addison-Wesley*, New York (1998).

10. G. R. Fowles. Introduction to Modern Optics. *Dover Publications* (2012).

11. F. L. Pedrotti, L. S. Pedrotti. Introduction to Optics. *Longman Higher Education* (1987).

12. R. Azzam, N. M. Bashara. Ellipsometry and Polarized Light. *North-Holland* (1988).